INTERNATIONAL JOURNAL OF CURRENT RESEARCH IN CHEMISTRY AND PHARMACEUTICAL SCIENCES

(p-ISSN: 2348-5213: e-ISSN: 2348-5221)
www.ijcrcps.com

Research Article

CRYSTALLOGRAPHIC AND MORPHOLOGICAL STUDY OF SODIUM ZIRCONIUM PHOSPHATE AS A HOST STRUCTURE FOR IMMOBILIZATION OF BARIUM

RASHMI CHOURASIA*, O. P. SHRIVASTAVA AND VIJAY VARMA

Department of Chemistry, Dr H.S.Gour University, Sagar, M.P. 470003, India
*Corresponding Author: dr.rchourasia@gmail.com

Abstract

Sodium zirconium phosphate (NZP) is a potential material for immobilization of nuclear effluents. The Structure of polycrystalline phase of barium containing NZP was determined on the basis of crystal data of solid state simulated waste forms. The crystal structure of $Na_{1-x}Ba_{x/2}Zr_2P_3O_{12}$ (x=0.1-1.0) has been investigated using General Structure Analysis System (GSAS) programming. The BaNZP phase crystallizes in the space group R-3c and Z=6. Powder diffraction data have been subjected to Rietveld refinement to arrive at a satisfactory structural convergence of R-factors. The unit cell volume and polyhedral (ZrO_6 and PO_4) distortion increases with rise in the mole % of Ba^{2+} in the NZP matrix. SEM, TEM and EDX analysis provide analytical evidence of barium in the matrix.

Keywords: Ceramic; powder XRD; Rietveld refinement; SEM; nuclear waste immobilization.

Introduction

The disposal of high level radioactive waste generated during reprocessing of spent fuel from nuclear reactors to recover actinides is a research problem of interest to nuclear scientists. Chemically and radiologically, reprocessed wastes are very complex in nature [Hawkins and Scheetz (1996)]. To minimize the potential adverse health impacts to people during the entire lifetime of the radio nuclides involved, nuclear waste must be carefully and properly managed. The nuclear-waste management technology involves generation, processing (treatment and packaging), storage, transport and disposal [Man-Sung, Linga (2000)]. In this context the solid-state chemistry and structure–property relationship of the nuclear waste forms needs to be understood thoroughly. While making choice of the host material for such applications, high crystallinity and low thermal expansion matrices are preferable [Petkov and Orlova (2003), Buvaneswari et. al. (2004), Roy et. al. (1983), Naik et. al. (2004), Lutze and Ewing (1988)]. The solid state reactivity of sodium zirconium phosphate and its capacity to fix the radwaste cations is a function of various physico-chemical parameters like crystallinity, particle size, surface area, chemical composition, processing temperature, processing route, bulk density, site of substitutions, ionic radii of the incoming effluent cations, etc. Compounds of the NZP family may be represented by the general crystallochemical formula (M1) $(M2)_3$ $\{[L_2(TO_4)_3]P^-\}_{3\infty}$ with the structure containing a three-dimensional network of corner-sharing LO_6 octahedra and TO_4 tetrahedra [Pet'kov (2001)]. The structural units consisting of two octahedra and three tetrahedra ($[L_2(TO_4)_3]P^-$) are connected to form ribbons parallel to c axis of the unit cell. These ribbons are linked together perpendicular to the c axis by TO_4 tetrahedra to build the three-dimensional framework. In NZP, four crystallographic sites with different co-ordination numbers allow substitutions by a variety of cations. Two kinds of cavities within this framework of ribbons are formed; the first cavity, which is a strongly distorted octahedral site M1, is situated between $[L_2\ (TO_4)_3]P^-$ units of the ribbons. The other site, M2, is situated between the ribbons of ZO_6 octahedra. In the NZP structure of formula $NaZr_2(PO_4)_3$, the M1 site is occupied by sodium ions (Na^+), the M2 site remains vacant, the L site is occupied by Zr^{4+} and the T site is occupied by P^{5+}. Two L positions can be populated either with the tri or the tetravalent cations. The replacing atoms in the center of the LO_6 octahedron and the TO_4 tetrahedron (a tetrahedral site normally occupied by P^{5+}) cause changes in the negative charge of the framework.This charge is compensated by the substitutions in positions M1 and M2. These positions can be filled with cations with valences ranging from +1 to +4. NZP materials are intresting because of high thermal, chemical and

radiation stability, ionic conductivity [Tamura (2001), (2002), Imanaka and Adachi (2002)], low coefficients of thermal expansion [Alami (1994), Heintz (1997)] and luminescent properties [Bakhous et. al. (1999), Masui (2006), Berry (2006)]. It is reported to accommodate about 42 elements (including most fission and activation products) of the periodic table and therefore, a suitable host for accommodating radioactive wastes [Scheetz et. al. (1994), Roy et. al. (1983), Gauglitz et. al. (1992)]. Besides identifying the limit of barium loading, present communication demonstrates the scientific feasibility of barium immobilization in the NZP matrix through an acceptable structure model based on the refinement of crystallographic data. It also investigates the crystallochemical changes due to matrix modification when a large cation like Ba^{2+} is substituted for sodium on M1 site of the NZP framework. Powder diffraction data and calculations of crystal cell parameters, crystal symmetry, isotropic thermal parameters and other structural factors provide a good data base for process development.

Materials and Methods

Ceramic route synthesis of $Na_{1-x}Ba_{x/2}Zr_2P_3O_{12}$ phases

Calculated quantities of AR grade Na_2CO_3, $BaCO_3$, ZrO_2 and $(NH_4)H_2PO_4$ for the stochiometry $Na_{1-x}Ba_{x/2}Zr_2P_3O_{12}$ (x=0.1, 0.5 and 1) were thoroughly mixed with about 10 ml of 1, 2, 3 propane triol to form a semisolid paste. The glycerol paste was gradually heated initially at 600ºC for 4 hours in a crucible. This initial heating is done to decompose Na_2CO_3 and $(NH_4)H_2PO_4$ with emission of carbon dioxide, ammonia and water vapors. The mixture was reground to micron size, pressed into pellets and sintered in a platinum crucible at 1200ºC for 12 hours. The process was repeated to get a polycrystalline dense material.

Characterization

The powder X-ray diffraction pattern has been recorded between 2θ=10º-90º on a Pan Analytical diffractometer (XPERT-PRO) using CuKα radiation at step size of 2θ=0.017º and a fixed counting time of 5 sec/step. Scanning electron microscopy (SEM) has been carried out on an electron microscope system (HITACHI S-3400) equipped with Thermonoran ultra dry detector facility for energy dispersive X-ray (EDX) analysis. Transmission Electron Microscopy (TEM) study was done with a PHILIPS CM200 analytical instrument operated between 20-200kV.

Results and Discussion

Rietveld refinement and crystallographic model of the phases

X-ray diffraction data show that solid solution of compositions $Na_{1-x}Ba_{x/2}Zr_2P_3O_{12}$ (x=0.1and 0.5) are isostructural to $NaZr_2(PO_4)_3$ [JCPDS Powder diffraction data file no. 71-0959 (2000)] although in case of x=0.5, a minror secondary phase of barium zirconium phosphate (*marked) begins to appear along with $NaZr_2(PO_4)_3$ (Fig. 1). BaNZP (barium sodium zirconium phosphate) crystallizes in the rhombohedral system (x=0.1, 0.5 in R-3c space group whreas x=1.0 in R-3). The conditions for the rhombohedral lattice: (i) - h+k+l=3n (ii) when h=0, l=2n and (iii) when k=0, l=2n have been verified for all reflections between 2θ=10º-90º. The intensity and positions of the diffraction pattern match with the characteristic pattern of parent compound sodium zirconium phosphate, which gives several prominent reflections between 2θ=13.98º-46.47º [JCPDS Powder diffraction data file no. 71-0959 (2000)]. The Rietveld [Rietveld (1969)] refinement of the step scan data was performed by the least square method using GSAS software [Larson and Von Dreele (2000)]. Assuming that BaNZP belongs to the Nasicon family, Zr, P and O atoms are in the *12c*, *18e* and *36f* Wyckoff positions respectively of the R-3c space group. In BaNZP phases the Na atoms were assumed to occupy the M_1 *(6b)* site while M_2 site *(18e)* remains vacant. The occupancies of Na and Ba atoms have been constrained according to their theoretical molar ratios. The structure refinement leads to rather good agreement between the experimental and calculated XRD pattern (Fig.2a) and yields acceptable reliability factors: RF^2, Rp and Rwp [Table 1] [Kojitani et. al. (2005)]. The normal probability plot for the histogram gives nearly a linear relationship indicating that the *Io* and *Ic* values for the most part are normally distributed.

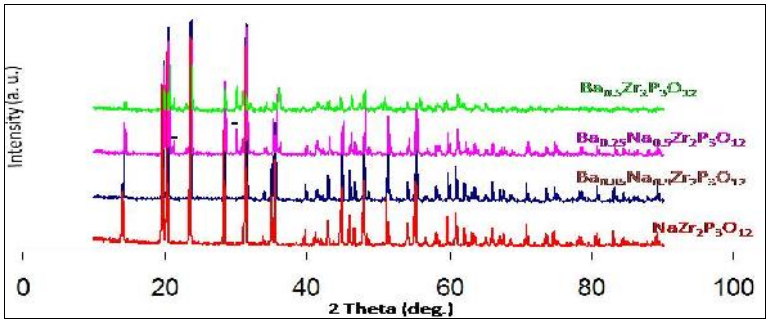

Fig. 1 Powder X-ray diffraction pattern of $Na_{1-x}Ba_{x/2}Zr_2P_3O_{12}$ (x=0.1-1.0) ceramic samples. Marked (*) are due to secondary phase of barium zirconium phosphate.

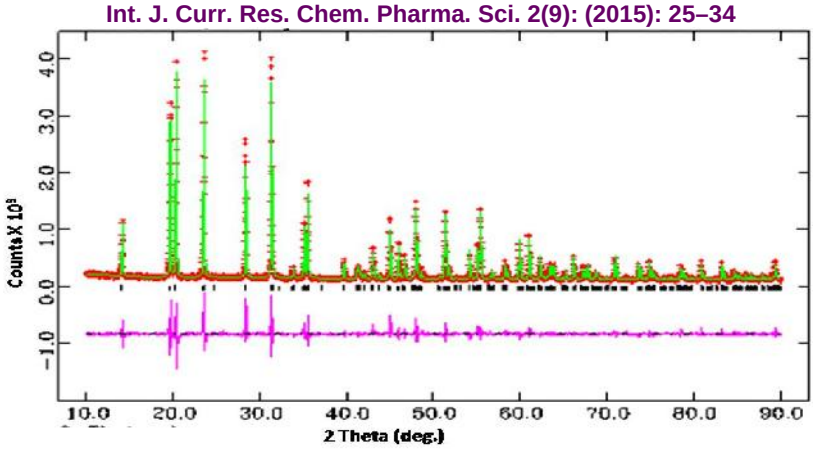

Figs. 2 Rietveld refinement plot for $Na_{0.9}Ba_{0.05}Zr_2P_3O_{12}$ ceramic sample showing observed (+), calculated (continuous line) and difference (lower) curves. The vertical bars denote Bragg reflections of the crystalline phases

The three-dimensional network structure of NZP consists of strongly bonded polyhedra, which imparts stability. The structure is flexible towards ionic substitutions on different available sites. The slight increase in lattice parameters may be explained as follows: Lattice parameter 'a' depends on the width of the ribbon and on the distance between the ribbons. These quantities are determined by number and size of phosphorus tetrahedrons and substituent cations. Crystal data reveals that the parateter 'a' as well as cell volume increases with increasing weight % of substituent cations between the ribbons.This behavior is due to expansion in the rhombohedral lattice caused by the substitution of a smaller Na^+ cation by larger Ba^{2+} cation (Table 1 and Fig. 3).

Table 1 Crystallographic data for $Na_{1-x}Ba_{x/2}Zr_2P_3O_{12}$ (x=0.1-1.0) phases

Structure	Rhombohedral
Space group	R-3c
Z	6
α = β =	90º
γ =	120.0º

Parameters	**X=0.1**	**X=0.5**	**X=1.0**
Lattice constants			
a= b	8.79326(7)	8.80260(30)	8.7355(9)
c	22.72401(30)	22.7666(14)	23.268(5)
Rp	0.0949	0.1469	0.1854
Rwp	0.1238	0.1966	0.2442
$R_{expected}$	0.0681	0.0697	0.0788
RF^2	0.08351	0.16872	0.20601
Volume of unitcell	1521.652(21)	1527.74(9)	1537.7(4)
S (GoF)	1.82	2.83	
DWd	0.832	0.431	0.241
Unit cell formula weight	2969.445	3079.065	3216.09
$Density_{X\text{-}ray}$	3.240	3.347	3.473

$$R_p = \frac{\sum y_i(obs) - y_i(cal)}{\sum y_i(obs)} \quad R_{wp} = \left\{ \frac{\sum w_i(y_i(obs) - y_i(cal))^2}{\sum w_i(y_i(obs))^2} \right\}^2 \quad R_e = \left[(N-P) / \sum w_i y_{oi}^2 \right]^{1/2} \quad S = R_{wp}/R_{exp}$$

$y_{i\,(o)}$ and $y_{i(c)}$ are observed and calculated intensities at profile point *i*, respectively. w*i* is a weight for each step *i*. N is the no of parameters refined.

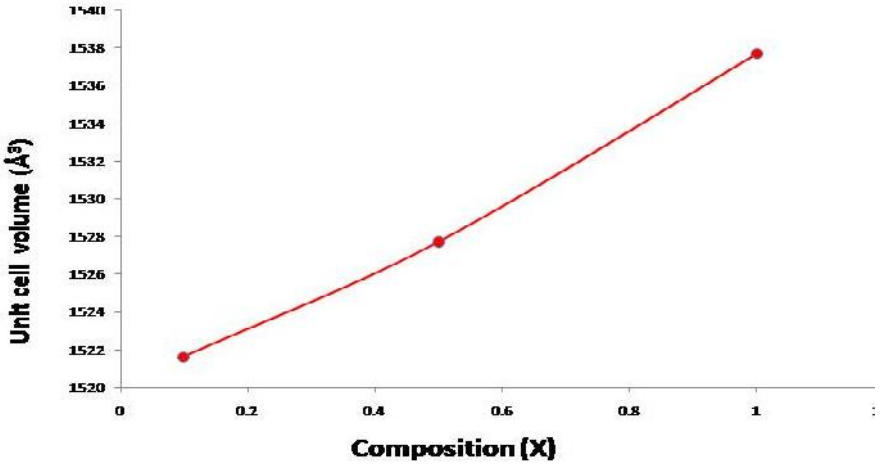

Fig. 3 Variation of unit cell volume with Ba loading in the $Na_{1-x}Ba_{x/2}Zr_2P_3O_{12}$ (x=0.1-1.0) solid solutions.

Alteration in lattice parameters shows that the network modifies its dimensions to accommodate the cations occupying M_1 site without breaking the bonds. The basic framework of NZP accepts the cations of different sizes and oxidation states to form solid solutions but at the same time retaining the overall geometry unchanged.The final atomic coordinates and isotropic thermal parameters (Table 2), inter-atomic distances, bond valencies (Table 3) and bond angles (Table 4) are extracted from the crystal information file prepared after final cycle of refinement. Selected h, k, l values, d-spacing, and intensity data along with observed and calculated structure factors have been listed in Appendix-I. The refinement leads to acceptable Zr-O, P-O bond distances. Zr atoms are displaced from the center of the octahedron due to the Na^{+}–Zr^{4+} repulsions. Consequently the Zr–O(2) distance, neighboring the sodium Na(1), is slightly greater than the Zr–O(1) distance, however, average Zr–O distances are smaller than the values calculated from the ionic radii data (2.12 Å) [Shannon and Prewitt (1969)]. The O–Zr–O angles vary between 76.90º and 176.3º. The angles implying the shortest bonds are superior to those involving the longest ones due to O-O repulsions which are stronger for O(1)-O(1) than for O(1)-O(2). The P-O distances are close to those found in Nascicon type phosphates.

Table 2 Refined atomic coordinates of polycrystalline $Na_{1-x}Ba_{x/2}Zr_2P_3O_{12}$ solid solutions at room temperature

Atom	x	y	z	Occupancy	$U_{isothermal}$ (Å^2)
$Na_{0.9}Ba_{0.05}Zr_2P_3O_{12}$					
Na	0.0	0.0	0.0	0.9	0.09597
Ba	0.0	0.0	0.0	0.05	0.09597
Zr	0.0	0.0	0.1456	1.0	0.03922
P	0.29111	0.0	0.25	1.0	0.04424
O1	0.17594	-0.02524	0.19628	1.0	0.04387
O2	0.1925	0.1742	0.08889	1.0	0.04387
$Na_{0.5}Ba_{0.25}Zr_2P_3O_{12}$					
Na	0.0	0.0	0.0	0.5	0.25071
Ba	0.0	0.0	0.0	0.25	0.25071
Zr	0.0	0.0	0.1456	1.0	0.04707
P	0.2911	0.0	0.25	1.0	0.04328
O1	0.17594	-0.02524	0.19628	1.0	0.06498
O2	0.1925	0.1742	0.08888	1.0	0.06498
$Ba_{0.5}Zr_2P_3O_{12}$					
Ba	0.0	0.0	0.0	1.0	0.23219
Zr	0.0	0.0	0.1488	1.0	0.06233
Zr	0.0	0.0	0.64577	1.0	0.06233
P	0.2928	0.008	0.2528	1.0	0.07017
O1	0.1971	0.0059	0.1961	1.0	0.13158
O2	0.0429	-0.1673	0.6939	1.0	0.13158
O3	0.183	0.1727	0.084	1.0	0.13158
O4	-0.169	-0.2097	0.5906	1.0	0.13158

Appendix-I Selected h, k, l values, d-spacing, observed and calculated structure factors and intensity of $Na_{0.9}Ba_{0.05}Zr_2P_3O_{12}$ ceramic phase. The reflection selected from the Crystallographic Information Framework (CIF) output of the final cycle of the refinement.

h	k	l	F^2_{Obs}	F^2_{Calc}	d-space	Intensity%
1	0	-2	19750.900	18287.684	6.32579	26.68
1	0	-2	19705.320	18287.684	6.32579	13.25
1	0	4	100894.91	96276.25	4.55351	76.30
1	0	4	98693.73	96276.25	4.55351	37.14
1	1	0	146054.17	146147.91	4.39663	93.92
1	1	0	141860.61	146147.91	4.39663	45.38
1	1	3	92472.18	85376.00	3.80250	100.00
1	1	3	87087.75	85376.00	3.80250	46.98
2	0	-4	157057.80	133768.83	3.16289	60.60
2	0	-4	162213.45	133768.83	3.16289	31.17
1	1	6	144558.28	137704.69	2.86949	99.85
1	1	6	141983.47	137704.69	2.86949	48.85
2	1	1	16422.938	16479.287	2.85546	10.66
2	1	1	16980.049	16479.287	2.85546	5.48
2	1	4	44952.10	41014.15	2.56754	24.21
2	1	4	44558.82	41014.15	2.56754	11.95
3	0	0	163043.14	160796.55	2.53840	42.77
3	0	0	158889.09	160796.55	2.53840	20.77
2	0	8	33574.082	33312.676	2.27675	8.04
1	1	9	12237.561	12853.434	2.18953	6.10
3	0	-6	50855.25	41969.38	2.10860	10.23
3	0	-6	50934.95	41969.38	2.10860	5.10
2	1	-8	66061.91	55503.40	2.02176	26.49
2	1	-8	64221.23	55503.40	2.02176	12.83
3	1	-4	40672.17	40191.24	1.97968	14.65
3	1	-4	40761.36	40191.24	1.97968	7.32
2	0	-10	54158.29	55099.45	1.95131	10.54
2	0	-10	52056.37	55099.45	1.95131	5.05
2	2	6	97497.90	97520.27	1.90125	35.07
2	2	6	94899.17	97520.27	1.90125	17.02
4	0	-2	29127.232	21005.186	1.87762	5.06
2	1	10	88151.66	88135.33	1.78354	30.30
2	1	10	86470.48	88135.33	1.78354	14.81
3	1	-7	14971.037	16508.191	1.77036	5.06
3	1	8	40181.12	42038.80	1.69489	12.69
3	1	8	34634.492	42038.80	1.69489	5.46
3	2	4	52431.03	49264.69	1.66987	15.48
3	2	4	55045.20	49264.69	1.66987	8.10
4	1	0	108684.36	106767.66	1.66177	31.26
4	1	0	105807.42	106767.66	1.66177	15.17
1	0	-14	59056.25	52011.84	1.58748	9.23
4	0	-8	40586.10	35953.32	1.58145	5.89
3	1	-10	62448.87	66093.79	1.54704	17.78
3	1	-10	59819.32	66093.79	1.54704	8.49
4	1	-6	38107.64	34187.605	1.52173	10.18
4	1	6	37340.63	33495.656	1.52173	9.97
2	0	14	75148.57	80355.43	1.49313	10.90
2	0	14	74247.44	80355.43	1.49313	5.37
5	0	-4	52550.51	52034.19	1.47109	6.66
3	3	0	53553.46	54088.37	1.46554	6.70
4	0	10	49115.77	47492.89	1.45933	6.53
2	1	-14	44987.59	43092.73	1.41383	12.01
2	1	-14	44978.82	43092.73	1.41383	5.99
4	2	-4	23923.008	21494.949	1.39507	5.63
3	2	10	26968.541	27129.773	1.38503	6.49

5	1	4	46479.21	47930.30	1.32973	10.56
5	1	4	45156.61	47930.30	1.32973	5.12
3	1	14	31945.063	33634.938	1.28699	7.45
6	0	0	91596.13	91045.13	1.26920	9.83
5	2	0	27567.639	23630.285	1.21941	5.53
3	2	-14	42234.57	36580.34	1.18913	9.11
5	2	6	26562.545	23945.154	1.16073	5.25
4	3	10	44575.38	38126.73	1.09653	8.54

Intensities less than 5% were omitted

Table 3 Interatomic distances (Å) and polyhedral distortions and bond valency variation of polycrystalline $Na_{1-x}Ba_{x/2}Zr_2P_3O_{12}$ ceramic phases

M-O bond length	$Na_{0.9}Ba_{0.05}Zr_2P_3O_{12}$ (X=0.1)	$Na_{0.5}Ba_{0.25}Zr_2P_3O_{12}$ (X=0.5)	$Ba_{0.5}Zr_2P_3O_{12}$ (X=1.0)
Zr1–O1	2.027910(10)*3	2.03059(6)*3	2.02231(20)*3
Zr1–O2	2.068680(10)*3	2.07281(7)*3	
Zr1–O3			2.16638(27)*3
Zr2–O2			2.01945(20)*3
Zr2–O4			2.11629(22)*3
P–O1	1.529830(10)*2	1.53216(6)*2	1.55707(26)
P–O2	1.520700(10)*2	1.52223(5)*2	1.54002(24)
P–O3			1.53008(15)
P–O4			1.50828(15)
Na1–O2	2.588220(20)*6	2.59065(10)*6	2.58849(4)*6
Ba–O3			2.4980(4)*6
Bond length distortion (Δ)			
$ZrO_6(\Delta x10^4)$	0.99	1.06	11.83
$PO_6(\Delta x10^6)$	0.89	1.05	5.13
Bond valences(V_i)			
Na1	0.81	0.80	4.10 (Zr1), 4.30
Zr	4.46	4.43	(Zr_2)
P	5.20	5.25	5.09

$\Delta = 1/n\ R\{(Ri - Rm)/(Rm)\}2$ where Ri individual bond length, Rm average bond length, and n number of coordinations

Vi = Rbij where bij = (Ro/R) N. where R is the bond length, N and Ro are constants (N=4.29 and Ro is the value of the bond length for unit bond valence).

Fig. 4 shows the PLATON projection of the molecular structure depicting the inter linking of ZrO_6 and PO_4 through a bridge oxygen atom. DIAMOND view illustrates the ZrO_6 inter ribbon distance in the structure of the title phase which is a function of amount and size of alkali cation in the M2 site of the 3D framework, built from ZrO_6 octahedrons and corner sharing PO_4 tetrahedrons. Substitution of Na^+ by larger cation of Ba^{2+} results in increase of distortion in ZrO_6 and PO_4 polyhedra. Calculated valences (Vi) [West (1984)] based on bond strength analysis [Shannon and Prewitt (1970), Breese and Keeffe (1991)] are in agreement with the expected oxidation states of Na^+, Zr^{4+} and P^{5+} respectively.

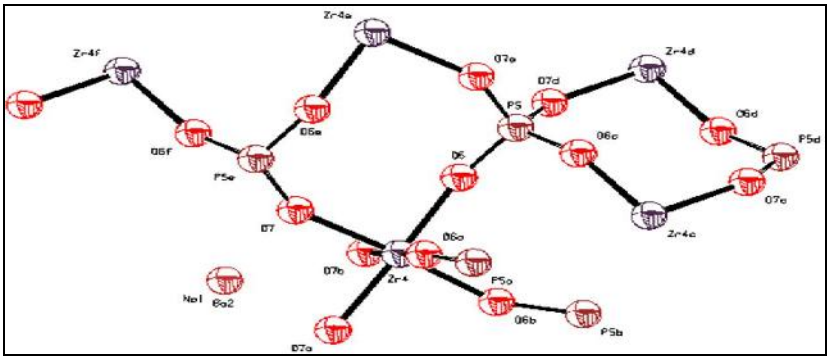

Fig. 4 PLATON view of molecular structure of $Na_{0.9}Ba_{0.05}Zr_2P_3O_{12}$ showing Zr coordination in ZrO_6 and P coordination in PO_4 polyhedron at 50% probability level.

Table 4 Interatomic bond angles (deg.) of polycrystalline $Na_{1-x}Ba_{x/2}Zr_2P_3O_{12}$ ceramic phases

O-M-O bond angles	***X=0.1***	***X=0.5***
O2−Na1−O2	65.5678(7)*6	65.5770(32)*6
O2−Na1−O2	180.0*3	180.0*3
O2−Na1−O2	114.4322(7)*6	114.4230(32)*6
O1−Zr−O1	90.8995(6)*3	90.8996(26)*3
O1−Zr−O2	92.7652(6)*3	92.8269(27)*3
O1−Zr−O2	175.8492(10)*3	175.8069(10)*3
O1−Zr−O2	90.9229(6)*3	90.9643(28)*3
O2−Zr−O2	85.2910(6)*3	85.1929(29)*3
O1−P−O1	107.7606(8)	107.812(4),
O1−P−O2	108.59470(10)*2	108.52830(30)
O1−P−O2	112.7430(4)*2	112.7932(17)*2
O2−P−O2	106.4906	106.4736
$Ba_{0.5}Zr_2P_3O_{12}$ (x-1.0)		106.4736
O3−Ba1−O3	65.271(11)*6	
O3−Ba1−O3	114.729(11)*6	
O3−Ba1−O3	180*3	
O1−Zr1−O1	93.195(9)*3	
O1−Zr1−O3	92.214(10)*3,96.793(10)*3,168.3552(5)*3	
O3−Zr1−O3	76.903(11)*3	
O2−Zr2−O2	92.218(9)*3	
O2−Zr2−O4	176.30580(30)*3, 90.660(30)*3, 89.984(10)*3	
O4−Zr2−O4	87.024(10)*3	
O1−P−O2	112.503(13)	
O1−P−O3	108.708(5)	
O1−P−O4	108.3039(17)	
O2−P−O3	106.5124(15)	
O2−P−O4	112.047(6)	
O3−P−O4	109.28160(10)	

*denotes multiplicity

SEM and TEM analysis

Within permissible statistical limits, the weight and atomic % of Na, Ba, Zr, P and O are agreeable with the EDX analysis. In $Na_{0.9}Ba_{0.05}Zr_2P_3O_{12}$ the wt% ratios Ba/Na was found to be 0.18 against the calculated value of 0.13. Likewise, the observed and calculated atomic ratios in this specimen are 0.17 and 0.11 respectively.The EDX spectra provide the evidence of barium in the polycrystalline mono phases while scanning electron micrographs show the rectangular parallelepiped crystallites of varying diameters between 0.5 and 6μm. (Fig. 5a and 5b).

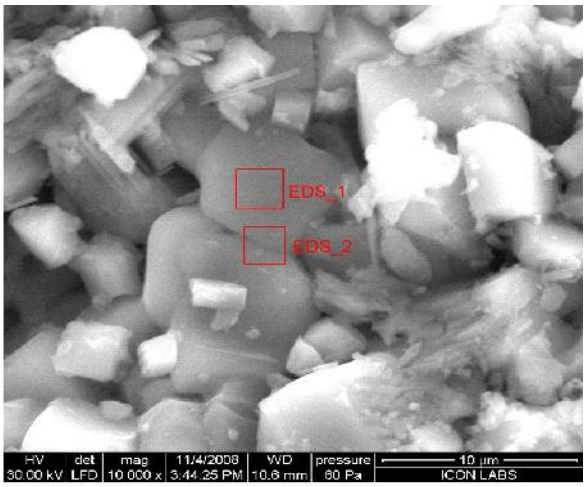

Fig. 5a

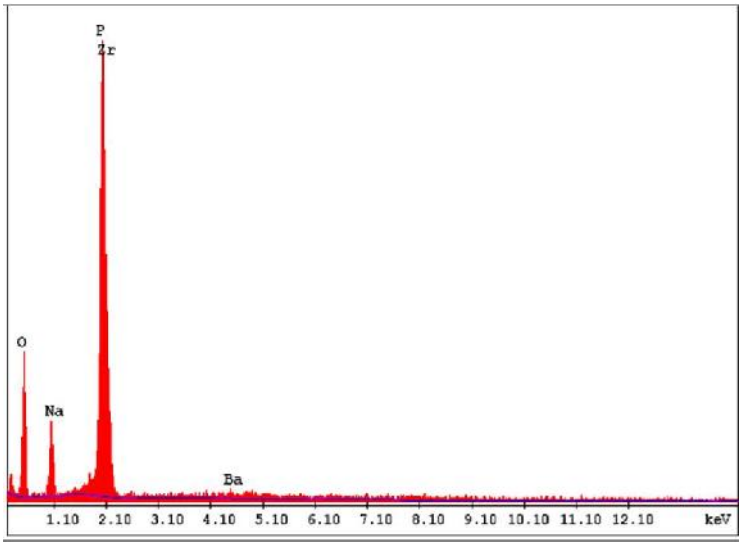

Fig. 5b

Figs. 5 (a) Scanning electron micrograpghs and **(b)** EDAX spectrum of $Na_{0.9}Ba_{0.05}Zr_2P_3O_{12}$ ceramic phase.

In TEM, the nano powder was observed in the form of agglomerates (Fig. 6a). Simultaneously, the particle size was also determined using the Scherrer's equation where broadening of peak is expressed as full width at half maxima (FWHM) in the recorded XRD pattern [West (1984)] (Table 5). The selected area electron diffraction (SAED) pattern of nano ceramic shows concentric rings in the diffraction pattern, which confirms the polycrystalline nature of the ceramic powder. Crystallographic planes and ordered arrangement of atoms is visible in the electron microscopy image (Fig. 6b)

.

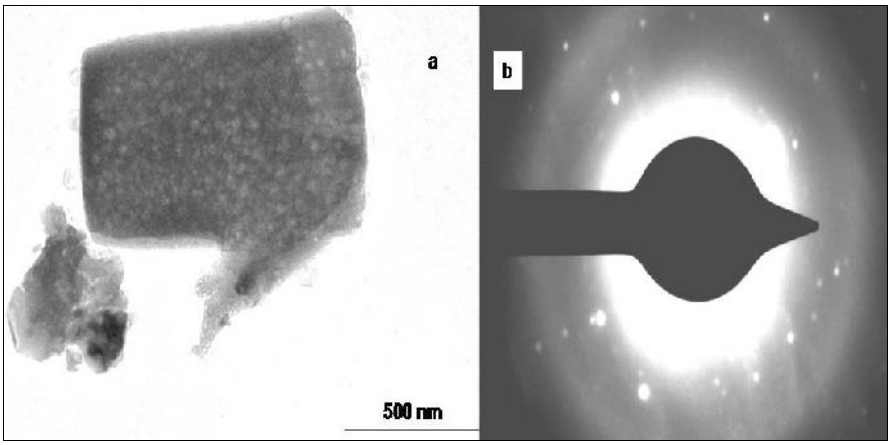

Fig. 6a 6b

Figs. 6(a) TEM image of the bulk nano phase of $Na_{0.9}Ba_{0.05}Zr_2P_3O_{12}$ **(b)** SAED image of $Na_{0.9}Ba_{0.05}Zr_2P_3O_{12}$ polycrystalline powder showing the fundamental reflections

Table 5 Distribution of particle size (nm) along prominent reflecting planes of $Na_{1-x}Ba_{x/2}Zr_2P_3O_{12}$ ceramic samples

h, k, l	X=0.1	X=0.5	X=1.0
1,0,-2	119.7	119.8	119.7
1,0,4	80.4	96.5	68.9
1,1,0	96.6	96.6	69.0
0,0,6	69.4	80.9	80.9
2,0,-4	98.1	98.1	70.0
116	123.4	123.4	61.8
214	99.7	124.7	99.8
300	124.8	124.8	83.2
30-6	166.6	125.07	63.4
21-8	105.4	140.6	128.5
3 1 -4	141.1	105.8	73.8
2 1 -10	141.5	141.5	64.8
2 2 6	85.3	106.7	104.1
2 1 10	108.1	108.1	21.9
3 1 8	87.5	109.5	66.7
3 2 4	109.9	109.9	67.1
4 1 0	109.5	146.8	67.1
3 1 -10	150.0	149.9	91.2
2 0 14	115.6	77.1	70.5

Conclusions

Refinement of powder X-ray diffraction data shows that the solid solutions of BaNZP (barium sodium zirconium phosphate) crystallizes in the rhombohedral system (x=0.1, 0.5 in R-3c space group whreas x=1.0 in R-3). The Rietveld plots represent a good structure fit between observed and calculated intensity with satisfactory R-factors. The bond distances Zr-O, P-O, Na-O are in agreement with their corresponding values for respective oxides. Cell volume and bond distortions in ZrO_6 and PO_4 polyhedra vary linearly with barium loading but the overall structure of the matrix remains intact. NZP has been identified as a potential material for immobilization and solidification of barium.

Acknowledgments

Authors are thankful to Prof J. P. Shrivastava, department of Geology, Delhi University, India for SEM/EDAX analysis and department of Metallurgical Engineering and Material Science I.I.T. Bombay, India for XRD analysis. One of the authors (Dr Rashmi Chourasia) is grateful to UGC, New Delhi, India for the award of Women Post Doctoral Fellowship.

References

Alami Talbi M., Brochu R., Parent C. 1994 The New Phosphates $Ln_{1/3}Zr_2(PO_4)_3$ (*Ln* = Rare Earth) J. Solid State Chem. 110:350.

Bakhous K., Cherkaoui F., Benabad A. 1999 Structural Approach and Luminescence Properties of $La_{1/6}Pb_{1/3}Zr_2(PO_4)_{17/6}(SiO_4)_{1/6}:Eu^{3+}$ J. Solid State Chem. 146: 499.

Berry Frank J., Costantini Nicola, Smart Lesley E. 2006 Synthesis and characterisation of Cr^{3+} containing NASICON-related phases, Solid State Ionics, 177: 2889–2896

Breese N. E., Keeffe M. O. 1991 Bond-valence parameters for solids, Acta Cryst. B47: 192.

Buvaneswari G., Govindan Kutty K.V., Varada-Raju U.V. 2004 Thermal expansion behaviour of sodium zirconium phosphate structure type phosphates containing tin. Mater. Res. Bull. 39: 475.

Gauglitz R., Holterdorf M., Marx G. 1992. In: Sombret, C.G. (Ed.), Scientific Basis for Nuclear Waste Management XV. Materials Research Society, Pittsburgh, PA, p. 567.

Hawkins H. T. and Scheetz B. E. 1996 Preparation of mono phasic Sodium Zirconium Phosphate (NZP) Radiophases: Potential Host Matrix for the immobilization of Reprocessed Commercial High-Level Wastes. Proceedings of the Material Research Society. fall meeting Boston. MA December 2-6.

Heintz J. M., Rabardel L., Qaraoui M. Al 1997 New low thermal expansion ceramics sintering and thermal behavior of $Ln_{1/3}Zr_2(PO_4)_3$ based composites. J. Alloy Compd. 250:515.

Imanaka N. and Adachi G.Y. 2002 Rare earth ion conduction in tungstate and phosphate solids J. Alloy Compd. 344: 137.

JCPDS Powder diffraction data file no. 71-0959, 2000 compiled by International Center for Diffraction Data U.S.A.

Kojitani H., Kido M., Akaogi M. 2005 Rietveld analysis of a new high-pressure strontium silicate $SrSi_2O_5$. Phys. Chem. Minerals. 32: 290.

Larson A. C., R.B. Von Dreele 2000 General Structure Analysis System technical manual, LANSCE, MS–H805. Los Almos National Laboratory LAUR, 86-748.

Lutze W. and Ewing R.C. 1988 Radio active waste for the future, Elsevier Science Publication. 238.

Man-Sung Yim, Linga K. Murty 2000 Materials issues in nuclear-waste management. Radioactive Waste Overview. JOM 5:26–29.

Masui T., Koyabu K., Tamura S. 2006 Synthesis of a new NASICON-type blue luminescent material. J. Alloy Compd. 418:73.

Naik A. H., Thakkar N. V., Dharwadkar S. R., Singh K. D. Mudher and Venugopal V. 2004 Journal of Thermal Analysis and Calorimetry. 78:707–713.

Pet'kov V.I., Dorokhova, G.I., Orlova, A.I. 2001 Architecture of phosphates with $\{[Li_2(PO_4)_3]p-\}_{3\infty}$ frameworks. Crystallogr. Rep. 46: 69–74.

Petkov V. I. and Orlova A. I. 2003 Crystal-chemical approach to predicting the thermal expansion of compounds in the NZP family. Inorg. Mater. 39(10): 1013–1023.

Rietveld H. M. 1969 A Profile Refinement Method for Nuclear and Magnetic Structures. J. Appl. Cryst. 2:65.

Roy R., Yang L.J., Alamo J, Vance E. R. 1983 In: Brookins, D.J. (Ed.), Scientific Basis for Nuclear Waste Management VI, Amsterdam, North-Holland, p. 15.

Shannon R.D., Prewitt C.D. 1969 Effective ionic radii in oxides and fluorides, Acta Crystallogr. Sect. B 25:925–946.

Shannon R. D. and Prewitt C. T. 1970 Revised values of effective ionic radii. Acta Crystallographica. 26:1046–1048.

Scheetz B.E., Agarwal D.K., Breval E., Roy R. 1994 Sodium Zirconium Phosphate as a host structure for nuclear waste management: a review. Waste Manage. 14 (6): 489–505.

Tamura S., Imanaka N. and Adachi G., 2001 The enhancement of trivalent ion conductivity in NASICON type solid electrolytes. J. Mater. Sci. Lett. 20: 2123.

Tamura S., Imanaka N. and Adachi G., 2002 Trivalent ion conduction in NASICON type solid electrolyte prepared by ball milling. Solid State Ion. 155: 767-771.

West A.R. 1984 Solid State Chemistry and Its Applications, John Wiley, New York.